Materials Chemistry and Physics 122 (2010) 595–601

Contents lists available at ScienceDirect

Materials Chemistry and Physics

journal homepage: www.elsevier.com/locate/matchemphys

New cadmium and rare-earth metal molybdates with scheelite-type structure

E. Tomaszewicz[a,*], S.M. Kaczmarek[b], H. Fuks[b]

[a] West Pomeranian University of Technology, Department of Inorganic and Analytical Chemistry, Al. Piastow 42, 71-065 Szczecin, Poland
[b] West Pomeranian University of Technology, Institute of Physics, Al. Piastow 17, 70-310 Szczecin, Poland

ARTICLE INFO

Article history:
Received 24 August 2009
Received in revised form 18 March 2010
Accepted 19 March 2010

Keywords:
Inorganic compounds
Annealing
Differential thermal analysis (DTA)
Infrared spectroscopy (IR)
Electron resonance

ABSTRACT

New cadmium and rare-earth metal molybdates with the formula $Cd_{0.25}RE_{0.50}MoO_4$ (RE = Pr, Nd, Sm–Dy) were synthesized by the solid-state reaction of $CdMoO_4$ with corresponding $RE_2(MoO_4)_3$. The obtained compounds crystallize in the scheelite-type structure. They were characterized here by XRD, DTA-TG, IR and EPR methods. The $Cd_{0.25}RE_{0.50}MoO_4$ compounds showed solubility in $CdMoO_4$ forming the $Cd_xRE_{2-2x}(MoO_4)_{3-2x}$ ($0.50 < x < 1.00$) solid solutions. It can be found from EPR measurements of the samples with volatile Gd^{3+} ions content, that Gd^{3+} ions can be located at sites of octahedral symmetry, and both temperature and gadolinium content have an influence on local magnetic interaction and relaxation processes of Gd^{3+} ions.

1. Introduction

Double molybdates and tungstates containing rare-earth ions are attractive laser host materials due to a very high stability of emission, high efficiency, long lifetime and low excitation threshold as well as excellent chemical and thermal durability in air. The diode pumped solid-state lasers based on these compounds demonstrate very high stability of emission of nano- or femtosecond pulses with high peak power. These lasers are used for optical and undersea communications, medical and eye-safe detecting, scientific researches and in military applications.

Fedorov and Tunik [1,2] examined reactivity of the $CdWO_4$ (the wolframite-type structure, space group $P2/c$ [3]) with $RE_2(WO_4)_3$. The authors obtained the following compounds in the $CdWO_4$–$La_2(WO_4)_3$ system: $CdLa_2(WO_4)_4$ and $CdLa_4(WO_4)_7$ [4]. Both compounds do not show any homogeneity region [4]. The authors [1,2] obtained two families of double tungstates with the following formulas for the RE = Pr–Ho lanthanides: $Cd_{0.40}RE_{0.40}WO_4$ (the molar ratio of $CdWO_4/RE_2(WO_4)_3$ – 2:1) and $Cd_{0.25}RE_{0.50}WO_4$ ($CdWO_4/RE_2(WO_4)_3$ – 1:1). The $Cd_{0.40}RE_{0.40}WO_4$ phases crystallize in the scheelite-type structure and melt congruently for RE = Pr-Eu or incongruently when RE = Gd-Ho [1,2]. The latter compounds crystallize in the monoclinic system, in a structure that is very similar to the one of scheelite-type. The homogeneity region of the $Cd_{0.40}RE_{0.40}WO_4$ (RE = Pr-Dy) phases is located in the range of about 40.00–60.00 mol.% of $RE_2(WO_4)_3$ and its width decreases, as the RE^{3+} radius decreases. The thermal stability of these compounds decreases analogically. [1,2,4]. The concentration tetrahedron of the CdO–WO_3–RE_2O_3–MoO_3 system with a position of the $Cd_{0.25}RE_{0.50}WO_4$ and $Cd_{0.40}RE_{0.40}WO_4$ compounds is shown in Fig. 1.

Our earlier studies on a reactivity of cadmium tungstate with some rare-earth metal tungstates ($RE_2W_2O_9$, RE_2WO_6) showed an existence of the following new cadmium and rare-earth tungstates: $Cd_{0.25}RE_{0.50}\square_{0.25}WO_4$ (RE = Nd, Sm, Eu, Gd, □ – statistical distributed vacancies in cation sublattice) [5], $CdPr_2W_2O_{10}$ [6], $CdRE_2W_2O_{10}$ (RE = Y, Nd, Sm–Er) [7]. The $Cd_{0.25}RE_{0.50}\square_{0.25}WO_4$ compounds were prepared via the solid-state reaction of $CdWO_4$ with $RE_2W_2O_9$ and they crystallize in the scheelite-type structure [5]. $Cd_{0.25}RE_{0.50}\square_{0.25}WO_4$ melt congruently for RE = Nd, Sm or incongruently when RE = Eu, Gd in the temperature range of 1391–1450 K [5]. The second type double tungstates with the general formula $CdRE_2W_2O_{10}$ were obtained from $CdWO_4$ and an adequate RE_2WO_6 trough the solid-state reaction also [6,7]. The $CdPr_2W_2O_{10}$ crystallizes in the orthorhombic system with cell parameters: $a = 0.68567(2)$ nm; $b = 1.4586(7)$ nm; $c = 0.84102(4)$ nm and is isostructural with other types of double praseodymium tungstates $MPr_2W_2O_{10}$ (M = Mn, Co) [6]. The other cadmium and rare-earth tungstates of $CdRE_2W_2O_{10}$ type crystallize in the monoclinic system and their anion sublattice is made of WO_4 tetrahedra [7]. The $CdRE_2W_2O_{10}$ compounds decompose in the solid-state above 1400 K [6,7]. EPR results obtained for $CdGd_2W_2O_{10}$ showed that an interaction between Gd^{3+} ions had mainly antiferromagnetic type [7].

As a continuation with respect to the earlier works, new families of cadmium and rare-earth molybdato-tungstates with the scheelite-type structure $Cd_{0.25}RE_{0.50}\square_{0.25}(MoO_4)_{0.25}(WO_4)_{0.75}$ (RE = Pr, Nd, Sm–Dy, □ – statistical distributed vacancies in

* Corresponding author. Tel.: +48 91 449 45 63; fax: +48 91 449 46 36.
E-mail address: tomela@zut.edu.pl (E. Tomaszewicz).

0254-0584/$ – see front matter © 2010 Elsevier B.V. All rights reserved.
doi:10.1016/j.matchemphys.2010.03.052

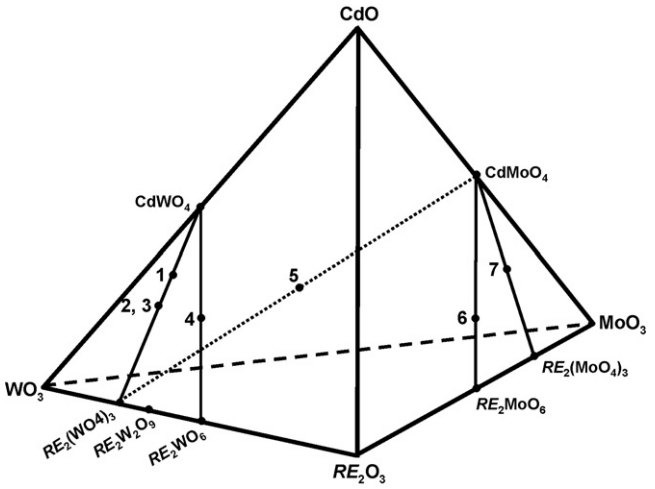

Fig. 1. Concentration tetrahedron of the $CdO–WO_3–RE_2O_3–MoO_3$ system 1 – $Cd_{0.40}RE_{0.40}WO_4$; 2 – $Cd_{0.25}RE_{0.50}WO_4$; 3 – $Cd_{0.25}RE_{0.50}\square_{0.25}WO_4$; 4 – $CdRE_2W_2O_{10}$; 5 – $Cd_{0.25}RE_{0.50}\square_{0.25}(MoO_4)_{0.25}(WO_4)_{0.75}$; 6 – $CdRE_4Mo_3O_{16}$; 7 – $Cd_{0.25}RE_{0.50}MoO_4$.

cation sublattice) [8] and the $Cd_xRE_{2-2x}(MoO_4)_x(WO_4)_{3-3x}$ solid solutions (*RE* = Pr, Nd, Sm–Dy) [9] were prepared and characterized by X-ray powder diffraction, infrared spectroscopy and thermal analysis techniques. It was found that the $Cd_{0.25}RE_{0.50}\square_{0.25}(MoO_4)_{0.25}(WO_4)_{0.75}$ phases melt congruently in the temperature range of 1382–1461 K [8]. The positions of the new cadmium and rare-earth tungstates and molybdatotungstates were marked in the concentration tetrahedron of the $CdO–WO_3–RE_2O_3–MoO_3$ system, seen in Fig. 1.

Cadmium and rare-earth metal molybdates $CdRE_4Mo_3O_{16}$ (*RE* = Y, La–Yb, Fig. 1) were prepared for the first time by Faurie and Kohlmuller who reported their XRD, IR, magnetic and luminescent data [10]. The $CdRE_4Mo_3O_{16}$ compounds were obtained by heating, in the solid-state, rare-earth metal molybdates RE_2MoO_6 with cadmium molybdate $CdMoO_4$ mixed at the molar ratio of 2:1 [10]. The compounds crystallize in the cubic space group *Pn*3*n* and their structure can be described as a derivative of the fluorite type structure with a tetrahedral environment of Mo^{6+} ions [11].

In the present paper, we describe synthesis and perform characterization of new cadmium and rare-earth metal molybdates $Cd_{0.25}RE_{0.50}MoO_4$ (*RE* = Pr, Nd, Sm–Dy) and the $Cd_xRE_{2-2x}(MoO_4)_{3-2x}$ ($0.50 < x < 1.00$) solid solutions using XRD, DTA-TG, IR and EPR methods. In order to characterize a nature of the magnetic interaction in this type of materials, EPR studies of $Cd_xGd_{2-2x}(MoO_4)_{3-2x}$ for $x = 0.50, 0.60, 0.70, 0.75, 0.80, 0.90, 0.975$ and 0.995 have been carried out in the temperature conditions from the ambient one to the one of liquid nitrogen.

2. Experimental

2.1. Synthesis

CdO, MoO_3, Pr_6O_{11} and other rare-earth metal oxides RE_2O_3 (all 99.9%, Aldrich) were used as starting materials. Cadmium molybdate ($CdMoO_4$) and rare-earth molybdates ($RE_2(MoO_4)_3$, *RE* = Pr, Nd, Sm–Dy) were prepared by the solid-state reactions. Heating was started from 823 K, stepwise increasing temperature up to 1148 K (to prepare the $RE_2(MoO_4)_3$) or 1273 K (to obtain the $CdMoO_4$) to avoid a loss of MoO_3 due to its evaporation. The solid-state synthesis took 84 h (7 × 12 h). The reaction mixtures were ground in an agate mortar after each 12 h period of the annealing for a better reactivity. The $RE_2(MoO_4)_3/CdMoO_4$ mixtures were prepared within the range of cadmium molybdate from 10.00 to 99.5 mol.%. All mixtures were heated in the atmosphere of static air, in 12 h cycles and at the following temperatures: 1023 K, 1073 K, 1123 K and 1173 K. Additionally, the $RE_2(MoO_4)_3/CdMoO_4$ (*RE* = Sm–Dy) were annealed at the temperatures: 1273 K, 1298 K and 1323 K. After each heating period, all samples were cooled slowly down to ambient temperature, ground and examined for their content by XRD method. After each heating cycle a mass of each sample was controlled.

2.2. Characterization of experimental methods

A routine phase analysis was conducted with an X-ray powder diffractometer (DRON-3) operating at 40 kV/20 mA, using CuKα radiation (λ = 0.15418 nm). The powder diffraction patterns were collected within the 2Θ range 10–45°, at the stepped scan rate 0.02° per step and the count time of 1 s per step. Data suitable for indexing procedure were collected in the 2Θ range 10–100° with a step size of 0.02 (2Θ) and counting time of 10 s for each step. The POWDER [12,13] and DICVOL [14,15] programs were used for indexing procedure.

Infrared spectroscopy data were collected on a Specord M80 spectrophotometer in the range of 300–1200 cm^{-1} using KBr pellets.

Thermogravimetric analysis was performed on a TA Instruments thermoanalyzer (Model SDT 2960) at the heating rate of 10 K min^{-1} to a maximum temperature of 1673 K and in the air atmosphere (gas flow 110 mL h^{-1}).

The EPR measurements were carried out with a conventional X-band Brücker ELEXSYS E500 CW spectrometer operating at 9.5 GHz with 100 kHz magnetic field modulation. Temperature dependence of the EPR spectra was registered in the range 85–295 K.

Chemical analysis of metallic elements' content was preformed for selected phases and equimolar mixtures of $RE_2(MoO_4)_3$ with $CdMoO_4$. The analyzed samples were melted with a mixture of Na_2CO_3 with K_2CO_3 (as flux). The resulting melt was dissolved in a hot dilute hydrochloric acid. The obtained precipitate of MoO_3 was used to determining of molybdenum content (gravimetric analysis). The filtrate obtained after separation of MoO_3 precipitate was used for determining of cadmium and rare-earth elements' contents by ICP-AES method (IY ULTRACE 238 spectrometer).

3. Results and discussion

3.1. Phases identification in the $RE_2(MoO_4)_3–CdMoO_4$ system

The XRD analysis' results of the samples obtained after the last heating cycle of $RE_2(MoO_4)_3/CdMoO_4$ mixtures indicate that initial compounds react with each other in the solid-state. The XRD analysis of the samples, whose initial mixtures contained up to 50.00 mol % of $CdMoO_4$, showed that two solid phases were found in the treated samples, viz. the compounds: $RE_2(MoO_4)_3$ and yet unknown $Cd_{0.25}RE_{0.50}MoO_4$. At the molar ratio 1:1 of the $RE_2(MoO_4)_3/CdMoO_4$ mixtures, both reactants reacted to produce a new cadmium and rare-earth metal molybdates:

$$CdMoO_{4(s)} + RE_2(MoO_4)_{3(s)} = 4Cd_{0.25}RE_{0.50}MoO_{4(s)} \quad (1)$$

It was observed that the XRD patterns of $Cd_{0.25}RE_{0.50}MoO_4$ consisted of peaks due to the scheelite-type lattice. The scheelite-type peaks were found also on powder diffraction patterns of the samples that were obtained after heating of $RE_2(MoO_4)_3/CdMoO_4$ mixtures comprising initially over 50.00 mol.% of $CdMoO_4$. The positions of the scheelite-type peaks that we observed were being shifted towards higher angles as the $CdMoO_4$ content increases. This fact indicates that the $Cd_{0.25}RE_{0.50}MoO_4$ compounds can form scheelite-type solid solutions with $CdMoO_4$. The formula of these solid solutions may be written as $Cd_xRE_{2-2x}(MoO_4)_{3-2x}$.

3.2. Composition determination

The chemical analysis of metallic elements' contents was performed for $Cd_{0.25}RE_{0.50}MoO_4$ (*RE* = Eu and Dy) and equimolar, initial mixtures of $RE_2(MoO_4)_3$ (*RE* = Eu and Dy) with $CdMoO_4$. The experimental and calculated contents of Mo, Cd and *RE* in analyzed phases and mixtures are shown in Table 1. Very similar experimental values of metallic elements' contents for $Cd_{0.25}RE_{0.50}MoO_4$ and initial $RE_2(MoO_4)_3/CdMoO_4$ mixtures confirm the validity of the proposed formula for new cadmium and rare-earth molybdates.

3.3. Characterization of $Cd_{0.25}RE_{0.50}MoO_4$ and the $Cd_xEu_{2-2x}(MoO_4)_{3-2x}$ solid solutions by XRD and IR methods

Powder diffraction patterns of $Cd_{0.25}RE_{0.50}MoO_4$ were subjected to indexing procedure. Table S1 (supplementary data) shows the

Table 1
Contents of Mo, Cd and *RE* in $Cd_{0.25}RE_{0.50}MoO_4$ and equimolar $RE_2(MoO_4)_3/CdMoO_4$ mixtures (*RE* = Eu and Dy).

Phase/mixture	Mo content wt %		Cd content wt %		*RE* content wt %	
	Exp.	Cal.	Exp.	Cal.	Exp.	Cal.
$Cd_{0.25}Eu_{0.50}MoO_4$	35.05	36.34	10.24	10.64	28.41	28.78
Equimolar $Eu_2(MoO_4)_3/CdMoO_4$ mixture	35.12		10.28		28.43	
$Cd_{0.25}Dy_{0.50}MoO_4$	35.31	35.63	10.05	10.44	35.35	35.63
Equimolar $Dy_2(MoO_4)_3/CdMoO_4$ mixture	35.28		10.12		35.38	

Table 2
Crystallographic characteristics of $CdMoO_4$ and $Cd_{0.25}RE_{0.50}MoO_4$.

Compound	*a* (nm)	*c* (nm)	*c*/*a*	*Z*	*V* (nm^3)	d_{exp} ($g\,cm^{-3}$)	d_{cal} ($g\,cm^{-3}$)	Reference
$Cd_{0.25}Pr_{0.50}MoO_4$	0.52734 (3)	1.1591 (9)	2.1982	4	0.32235 (9)	5.26	5.32	This work
$Cd_{0.25}Nd_{0.50}MoO_4$	0.52537 (2)	1.1541 (3)	2.1968	4	0.31855 (7)	5.34	5.42	This work
$Cd_{0.25}Sm_{0.50}MoO_4$	0.52242 (8)	1.1475 (1)	2.1965	4	0.31319 (1)	5.50	5.58	This work
$Cd_{0.25}Eu_{0.50}MoO_4$	0.52146 (4)	1.1467 (1)	2.1990	4	0.31181 (8)	5.57	5.62	This work
$Cd_{0.25}Gd_{0.50}MoO_4$	0.52037 (1)	1.1430 (2)	2.1965	4	0.30951 (4)	5.65	5.72	This work
$Cd_{0.25}Tb_{0.50}MoO_4$	0.51881 (7)	1.1391 (7)	2.1957	4	0.30663 (1)	5.71	5.79	This work
$Cd_{0.25}Dy_{0.50}MoO_4$	0.51742 (4)	1.1357 (4)	2.1950	4	0.30406 (8)	5.79	5.88	This work
$CdMoO_4$	0.51557 (8)	1.1210 (9)	2.1744	4	0.29800 (9)	6.05	6.07	This work
$CdMoO_4$	0.5156 (1)	1.1196 (1)	2.1715	4			6.078	[3]

indexing results of these compounds. The calculated parameters of unit cells, the values of experimental (obtained by degassing of samples and hydrostatic weighing in pycnometric liquid – CCl_4) and calculated density for $Cd_{0.25}RE_{0.50}MoO_4$ and $CdMoO_4$ are shown in Table 2. The data tabulated in Tables S1 and Table 2 testify that $Cd_{0.25}RE_{0.50}MoO_4$ crystallize in the scheelite-type structure. The lattice parameters of these compounds linearly decrease, as the atomic number of a lanthanide increases (Fig. 2). Table 3 shows the calculated unit cells parameters for $Cd_{0.25}Eu_{0.50}MoO_4$, the $Cd_xEu_{2-2x}(MoO_4)_{3-2x}$ solid solutions (for $x = 0.60$; 0.70; 0.75; 0.80; 0.90) and $CdMoO_4$. As one can see, the parameters of unit cell for the solid solutions decrease linearly, as the $CdMoO_4$ content increases (see also Fig. 3).

Fig. 4 shows IR spectra of the $Cd_{0.25}RE_{0.50}MoO_4$. The fundamental frequencies of the MoO_4^{2-} anions (the scheelite-type structure, space group C_{4h}^6) in an aqueous solutions are: 894 cm^{-1} (ν_1), 407 cm^{-1} (ν_2), 833 cm^{-1} (ν_3) and 318 cm^{-1} (ν_4) [16,17]. The stretching multiples (ν_1 and ν_3) appear for solid molybdates with isolated MoO_4 tetrahedra in the vibration frequencies of 908–675 cm^{-1} as well as bending modes (ν_2 and ν_4) in the 440–260 cm^{-1} range [12–14]. In the light of literature information concerning IR spectroscopy of single and double molybdates with the scheelite-type structure [16–18] the absorption bands observed in the IR spectra of $Cd_{0.25}RE_{0.50}MoO_4$ with their maxima at 912 cm^{-1} are due to the symmetric stretching modes of Mo–O bonds in MoO_4. However, the broad absorption bands centered around 830 cm^{-1} and 716 cm^{-1} could be related to the asymmetric stretching vibrations of Mo–O bonds in MoO_4. On the other hand, the absorption bands with maxima located at around 440 cm^{-1} and 320 cm^{-1} can be assigned to the symmetric and asymmetric deformation modes of Mo–O bonds in MoO_4 tetrahedra, respectively [16–18].

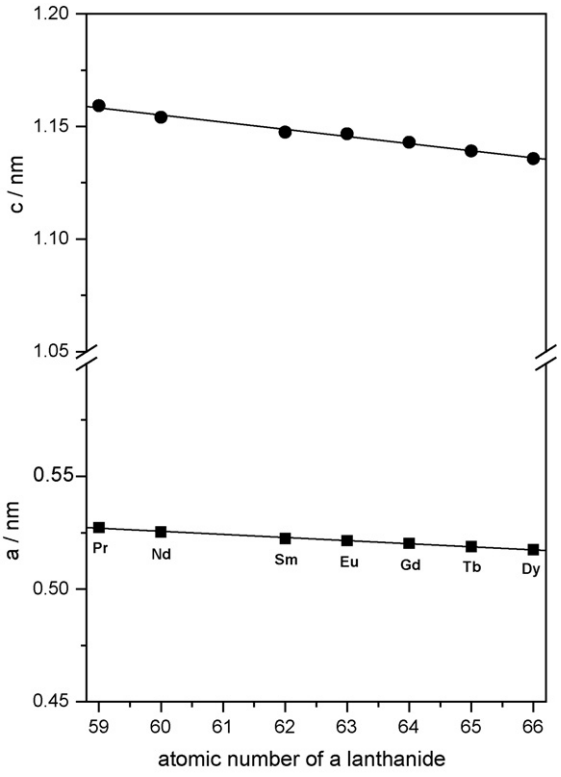

Fig. 2. Dependence of $Cd_{0.25}RE_{0.50}MoO_4$ cell parameters on the atomic number of a lanthanide.

Table 3
Crystallographic characteristics of $CdMoO_4$, $Cd_{0.25}Eu_{0.50}MoO_4$ and the $Cd_xEu_{2-2x}(MoO_4)_{3-2x}$ solid solutions for $x = 0.60$; 0.70; 0.75; 0.80 and 0.90.

Phase/Composition of initial $RE_2(MoO_4)_3/CdMoO_4$ mixture)	*a* (nm)	*c* (nm)	*c*/*a*	Reference
$Cd_{0.25}Eu_{0.50}MoO_4$ ($Cd_{0.50}Eu(MoO_4)_2$)	0.52146 (4)	1.1467 (1)	2.1990	This work
$Cd_{0.60}Eu_{0.80}(MoO_4)_{1.80}$ (40.00 mol.%. $Eu_2(MoO_4)_3$ + 60.00 mol.% $CdMoO_4$)	0.52098 (1)	1.1442 (1)	2.1963	This work
$Cd_{0.70}Eu_{0.60}(MoO_4)_{1.60}$ (30.00 mol.% $Eu_2(MoO_4)_3$ + 70.00 mol.% $CdMoO_4$)	0.52003 (5)	1.1402 (4)	2.1926	This work
$Cd_{0.75}Eu_{0.50}(MoO_4)_{1.50}$ (25.00 mol.% $Eu_2(MoO_4)_3$ 75.00 mol.% $CdMoO_4$)	0.51954 (8)	1.1375 (9)	2.1896	This work
$Cd_{0.80}Eu_{0.40}(MoO_4)_{1.40}$ (20.00 mol.% $Eu_2(MoO_4)_3$ + (80.00 mol.% $CdMoO_4$)	0.51907 (7)	1.1314 (6)	2.1798	This work
$Cd_{0.90}Eu_{0.20}(MoO_4)_{1.20}$ (10.00 mol.% $Eu_2(MoO_4)_3$ 90.00 mol.% $CdMoO_4$)	0.51770 (1)	1.1266 (7)	2.1763	This work
$CdMoO_4$	0.51557 (8)	1.1210 (9)	2.1744	This work

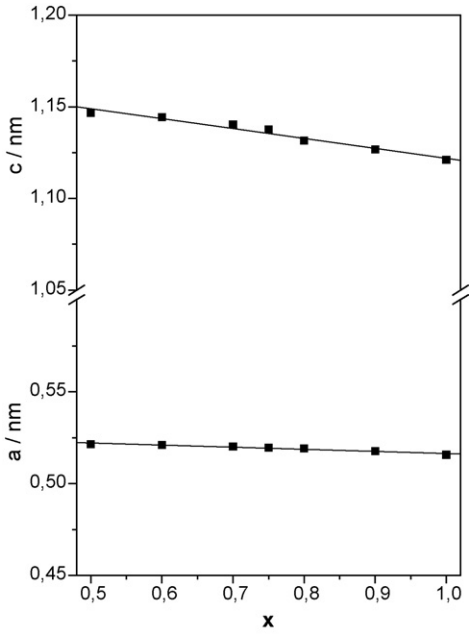

Fig. 3. Dependence of cell parameters of the $Cd_xEu_{2-2x}(MoO_4)_{3-2x}$ solid solutions on $CdMoO_4$ content.

3.4. Thermal studies of $Cd_{0.25}RE_{0.50}MoO_4$ and the $Cd_xEu_{2-2x}(MoO_4)_{3-2x}$ solid solutions

Fig. 5 shows DTA curves of $Cd_{0.25}RE_{0.50}MoO_4$ for *RE* = Pr and Dy. Only one endothermic effect was recorded up to 1673 K on each DTA curve. No mass losses were recorded on the TG curves (not presented) up to the onsets of the observed effects on the DTA curves. On the base of DTA studies performed for $Cd_{0.25}RE_{0.50}MoO_4$ and observations of the residues arising in corundum crucibles after these examinations it was found that the effects with their onsets at: 1291 K (Pr); 1317 K (Nd); 1331 K (Sm); 1340 K (Eu); 1354 K (Gd); 1348 K (Tb) and 1354 K (Dy) are connected with congruent melting of these compounds. Separate $Cd_{0.25}RE_{0.50}MoO_4$ samples were heated in a furnace for 4 h at a temperature selected from a range onset-minimum of each observed endothermic effect. After heating, the samples were quickly quenched to 263 K and next examined by XRD method. The diffraction patterns of the samples obtained by this way contained only diffraction lines with very low intensities that could be attributed to the starting materials.

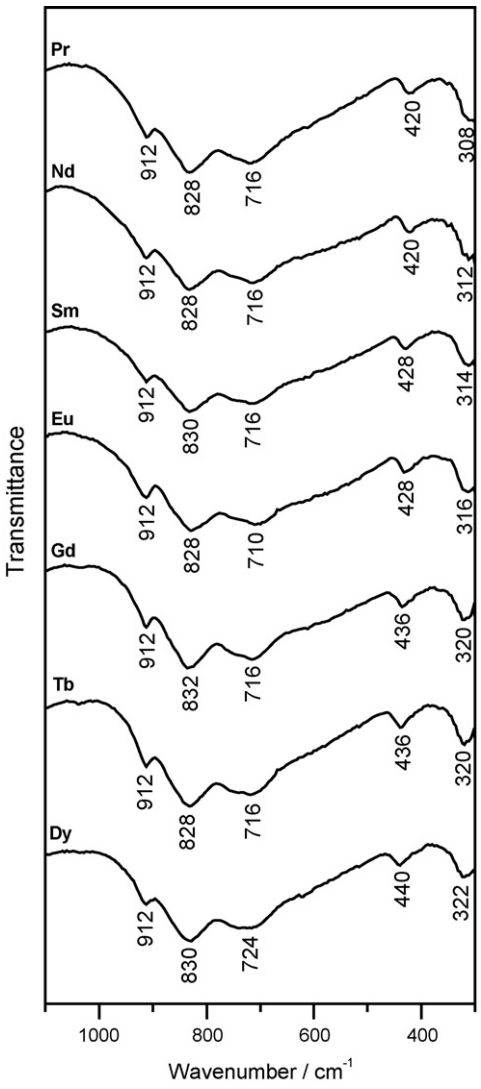

Fig. 4. IR spectra of $Cd_{0.25}RE_{0.50}MoO_4$.

This fact confirms congruent melting of the $Cd_{0.25}RE_{0.50}MoO_4$ compounds. Fig. 6 shows DTA curves of the $Cd_xEu_{2-2x}(MoO_4)_{3-2x}$ solid solutions for $x = 0.60$ and 0.90. The melting point of the obtained solid solutions increases linearly, as the $CdMoO_4$ content increases (Fig. 7).

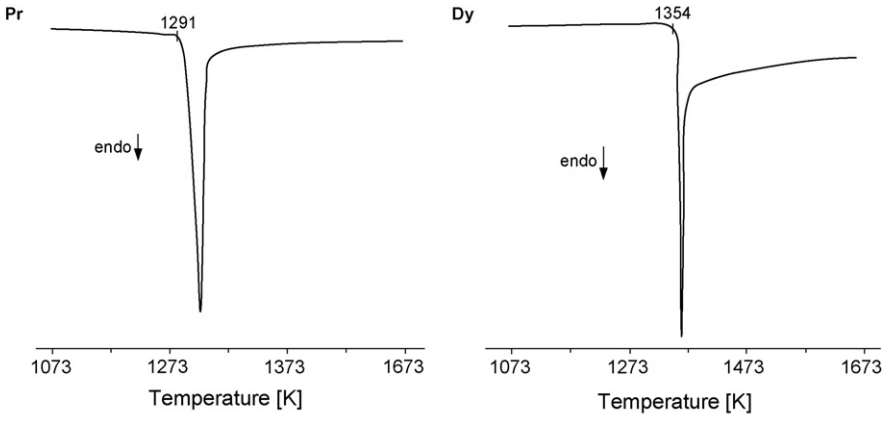

Fig. 5. DTA curves of the $Cd_{0.25}RE_{0.50}MoO_4$ compounds (*RE* = Pr and Dy).

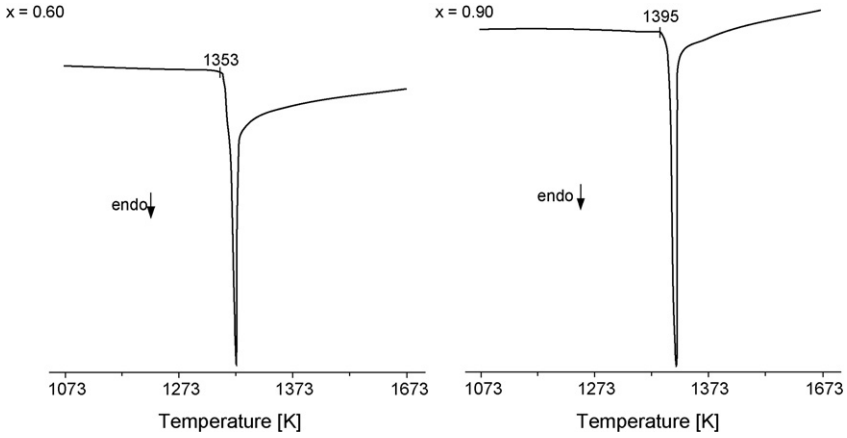

Fig. 6. DTA curves of the $Cd_xEu_{2-2x}(MoO_4)_{3-2x}$ solid solutions ($x = 0.60$ and 0.90).

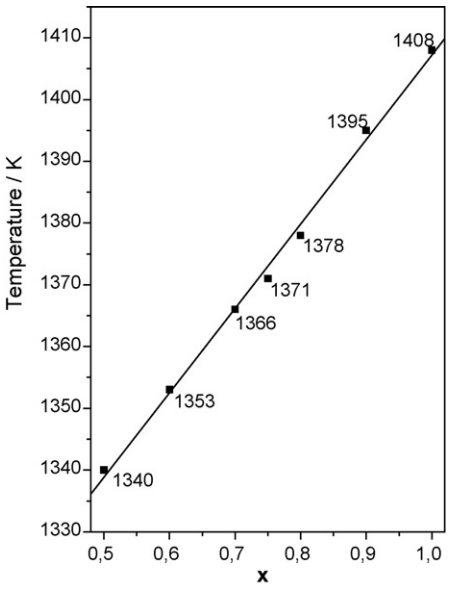

Fig. 7. Composition dependence of melting point for the $Cd_xEu_{2-2x}(MoO_4)_{3-2x}$ solid solutions.

3.5. EPR studies of $Cd_{0.25}Gd_{0.50}(MoO_4)$ and $Cd_xGd_{2-2x}(MoO_4)_{3-2x}$ solid solutions

The powder sample of $Cd_{0.25}Gd_{0.5}(MoO_4)$ has been investigated for temperature dependencies of its EPR signal in the range of 85–295 K. The observed resonance spectrum reveals a wide and intense EPR line attributed to the Gd^{3+} paramagnetic centers. The Gaussian shape of the EPR line (Fig. 8a) indicates on significant dipole–dipole interactions between gadolinium ions. The integral intensity of the line, I, as a function of a temperature one can describe by using the Curie–Weiss law $I = C/(T - \theta)$, revealing strong ferromagnetic interactions between Gd^{3+} ions with characteristic temperature parameter $\theta = 38$ K (Fig. 8b). Moreover, as a temperature increases from 85 K, the EPR line changes both: its width and resonance position (Fig. 9). This confirms that internal magnetic field and relaxation processes of Gd^{3+} paramagnetic centers are strongly temperature dependent in this case.

Fig. 10 shows an evolution of the EPR signal (at 120 K) with increasing of the Gd^{3+} content in $Cd_xGd_{2-2x}(MoO_4)_{3-2x}$ ($0.50 < x < 1.00$) samples. For extremely low concentration of the gadolinium ions (lowest line), the EPR spectrum is very complex and enough good resolved, as is expected for the resonance of the $S = 7/2$ state of Gd^{3+} ion, split by local crystal field. At higher Gd^{3+} concentration the exchange interaction between paramagnetic ions becomes more significant and EPR signal is broadened,

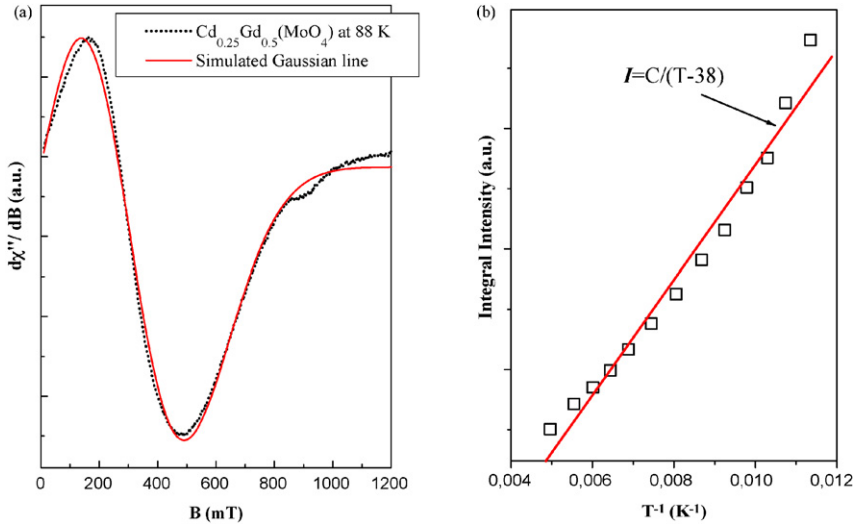

Fig. 8. (a) EPR spectrum of the $Cd_{0.25}Gd_{0.5}(MoO_4)$ at a temperature of 88 K, (b). The integral intensity of the Gd^{3+} EPR line as a function of inverse temperature for $Cd_{0.25}Gd_{0.5}(MoO_4)$.

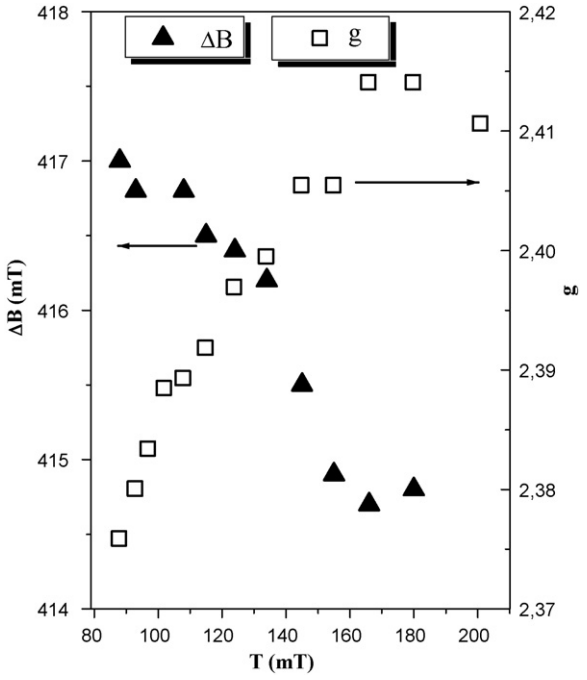

Fig. 9. Temperature dependence of EPR peak-to-peak linewidth (triangles) and effective g- spectroscopic parameter (squares) for Gd^{3+} ions in $Cd_{0.25}Gd_{0.5}(MoO_4)$.

forming a wide line (upper spectrum). All the investigated samples were weighted in order to evaluate the relative intensity of the signal. For all samples the integral intensity obeyed Curie–Weiss law and revealed significant ferromagnetic interactions between Gd^{3+} ions with positive parameter $\theta \approx 16$ K.

At lower gadolinium concentration, the EPR signal has rather asymmetric shape (Fig. 11), while with increasing the Gd^{3+} content the line becomes more symmetric (Fig. 12). The simulated lines are also shown in both figures. The simulation of the EPR signal was performed for a temperature of c.a. 120 K by using the EPR-NMR program [19]. The results, including linewidth, spectroscopic g parameter, some crystallographic parameters and relative intensity of a signal are collected in Table 4.

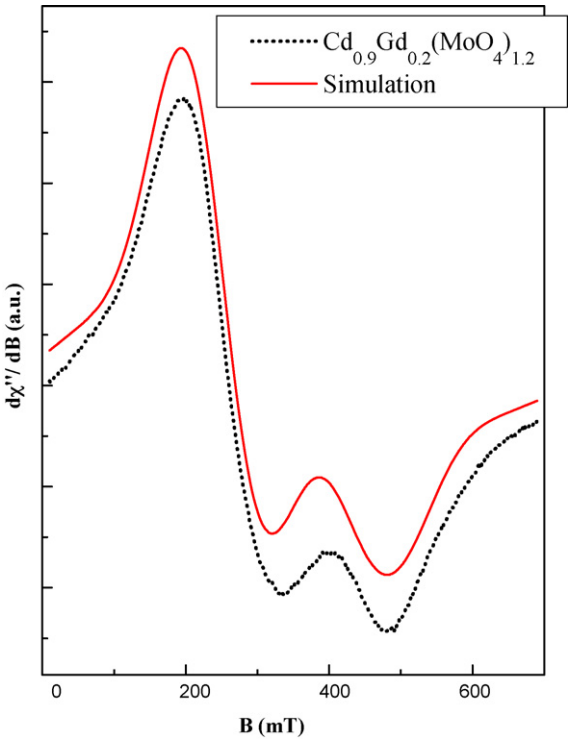

Fig. 11. EPR spectrum of Gd^{3+} ions in $Cd_{0.9}Gd_{0.2}(MoO_4)_{1.2}$ and simulated line (T = 120 K).

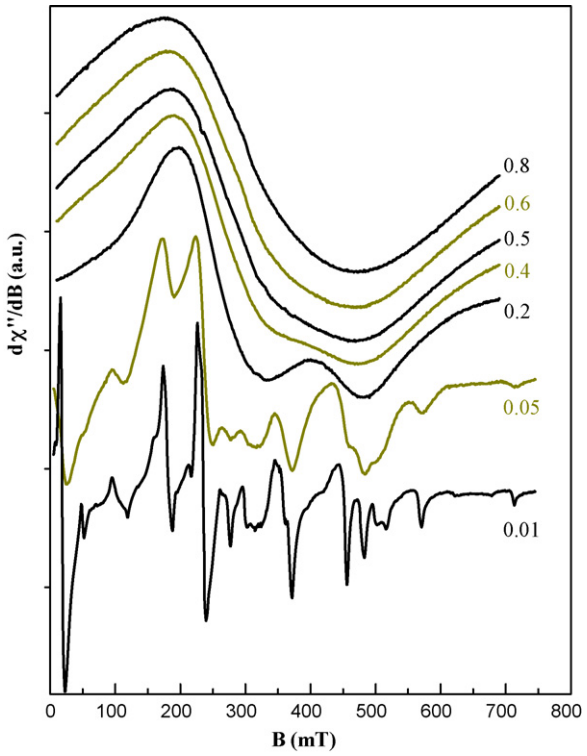

Fig. 10. EPR signals for $Cd_xGd_{2-2x}(MoO_4)_{3-2x}$ samples measured at 120 K with different Gd^{3+} concentration ($2-2x$), from 0.01 to 0.8.

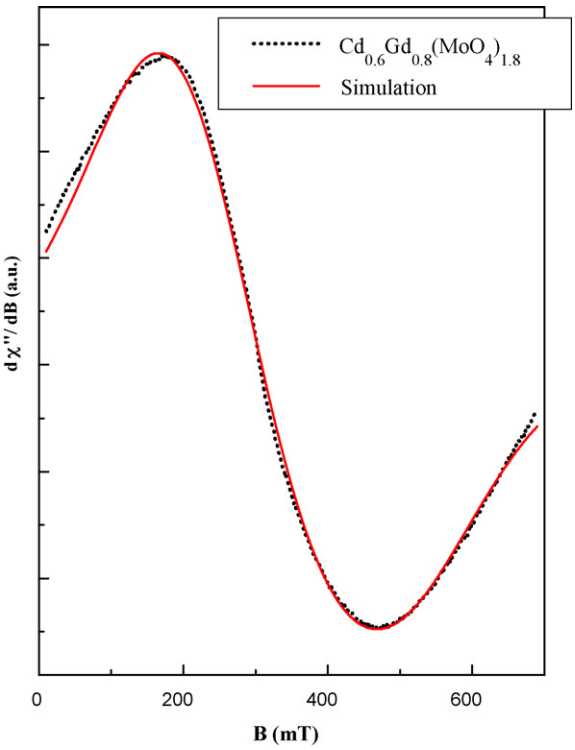

Fig. 12. EPR spectrum of Gd^{3+} ions in $Cd_{0.6}Gd_{0.8}(MoO_4)_{1.8}$ and simulated line (T = 120 K).

Table 4
The linewidth, ΔB, g-factor, D, B_4^0 – spin Hamiltonian parameters and $I/I_{0.2}$ – relative intensity of EPR signal for different concentration of Gd^{3+} ions.

$2-2x$	ΔB (Gauss)	g	D (Gauss)	B_4^0 (Gauss)	$I/I_{0.2}$
0.2	1050	1.950	750	−0.5	1
0.4	1400	1.945	720	−0.55	1.74
0.5	1500	1.945	720	−0.55	1.80
0.6	1650	1.940	720	−0.6	2.28
0.8	2100	1.925	720	−0.65	1.95

The best fitting we obtained for spin Hamiltonian including no higher than forth order crystal field parameters (Stevens operators), where just B_4^0 has the significant meaning. So, spin Hamiltonian applied to Gd^{3+} ions in this case had the form:

$$H_s = \mu_B BgS + D\,[S_Z^2 - 1/3\,S(S+1)] + E\,(S_x^2 - S_y^2) + B_4^0 O_4^0 \qquad (2)$$

with insignificant rhombic distortion represented by E parameter, i.e. $E \sim 0$. Other parameters of the above equation have their usual meaning.

As it could be seen from Table 4, the internal magnetic field, relaxation processes and local crystal field depend in some extent on the gadolinium content. B_4^0 parameter suggests that Gd^{3+} ions can have local octahedral surrounding in the compounds with no rhombic distortion ($E \sim 0$).

4. Conclusions

New cadmium and rare-earth metal molybdates with the formula $Cd_{0.25}RE_{0.50}MoO_4$ (RE = Pr, Nd, Sm–Dy) were prepared by the solid-state reaction between $CdMoO_4$ and $RE_2(MoO_4)_3$. The obtained phases are isostructural and crystallize in the scheelite-type structure. All compounds melt congruently in the temperature range of 1291–1354 K. Their melting points are lower than melting points or temperature of decomposition of obtained previously cadmium and rare-earth metal tungstates $Cd_{0.25}RE_{0.50}\square_{0.25}WO_4$, $CdRE_2W_2O_{10}$, and cadmium and rare-earth metal molybdato-tungstates $Cd_{0.25}RE_{0.50}\square_{0.25}(MoO_4)_{0.25}(WO_4)_{0.75}$. The $Cd_{0.25}RE_{0.50}MoO_4$ phases can form solid solutions with $CdMoO_4$ with the general formula $Cd_xRE_{2-2x}(MoO_4)_{3-2x}$ for $0.50 < x < 1.00$. EPR measurements performed for the samples with volatile content of Gd^{3+} have shown that Gd^{3+} ions can be located at octahedral positions. Both, temperature and gadolinium content have an influence on a kind of local magnetic interaction and relaxation processes of Gd^{3+} ions. A significant dipole-dipole interaction dominates between Gd^{3+} ions.

Appendix A. Supplementary data

Supplementary data associated with this article can be found, in the online version, at doi:10.1016/j.matchemphys.2010.03.052.

References

[1] T.A. Tunik, N.F. Fedorov, Zh. Neorgan. Khim. 26 (1981) 1884 (in Russian).
[2] N.F. Fedorov, T.A. Tunik, L.A. Burba, Zh. Neorgan. Khim. 21 (1976) 779 (in Russian).
[3] M. Daturi, G. Busca, M.M. Borel, A. Leclaire, P. Piaggio, J. Phys. Chem. B 101 (1997) 4358.
[4] A.A. Evdokimov, V.A. Ephremov, V.K. Trunov, I.A. Klejnman, B.F. Dzhyrinskij, Soedineniya Redkozemenykh Elementov. Molibdaty, volframaty. Nauka, Moskva, 1991. (in Russian).
[5] E. Tomaszewicz, S.M. Kaczmarek, H. Fuks, J. Rare Earths 27 (2009) 569.
[6] E. Tomaszewicz, J. Therm. Anal. Calorim. 93 (2008) 711.
[7] E. Tomaszewicz, S.M. Kaczmarek, Rev. Adv. Mater. Sci. 23 (2010) 88.
[8] E. Tomaszewicz, G. Dąbrowska, J. Therm. Anal. Calorim, in press, doi:10.1007/s10973-010-0776-y.
[9] E. Tomaszewicz, G. Dąbrowska, S.M. Kaczmarek, H. Fuks, J. Non-Cryst. Solids, in press.
[10] J.P. Faurie, R. Kohlmuller, Rev. Chim. Miner. 8 (1971) 241.
[11] J.B. Bourdet, R. Chevalier, J.P. Fournier, R. Kohlmuller, J. Omaly, Acta Crystallogr. B38 (1982) 2371.
[12] D. Taupin, J. Appl. Crystallogr. 1 (1968) 87.
[13] D. Taupin, J. Appl. Crystallogr. 6 (1973) 380.
[14] D. Louer, M. Louer, J. Appl. Crystallogr. 5 (1972) 271.
[15] A. Boultif, D. Louer, J. Appl. Crystallogr. 24 (1991) 987.
[16] R.G. Brown, J. Denning, A. Hallett, S.D. Ross, Spectrochim. Acta 26A (1970) 963.
[17] G.M. Clark, W.P. Doyle, Spectrochim. Acta 22 (1966) 1441.
[18] J. Hanuza, M. Mączka, J.H. van der Maas, J. Mol. Struct. 348 (1995) 349.
[19] M.J. Mombourquette, J.A. Weil, D.G. McGavin, EPR-NMR User's Manual, Department of Chemistry, University of Saskatchewan, Saskatoon, SK, Canada, 1999.